Materials Research. 2020; 23(1): e20190539
DOI: https://doi.org/10.1590/1980-5373-MR-2019-0539

Effect of Zr Content on the Distribution Characteristic of the 14H and 18R LPSO Phases

***Wanneng Zhang*[a], *Zhongxue Feng*[a]*, *Xu Li*[a], *Yuming Chen*[a]**

[a]*Kunming University of Science and Technology, School of Materials Science and Engineering, Kunming, 650093, China*

Received: September 25, 2019; Revised: October 17, 2019; Accepted: November 11, 2019

Zirconium (Zr) is an essential element in Mg-Zn and Mg-Zn-Y system magnesium alloys. In this study, an interesting phenomenon that the content of Zr element could influence the size and the morphology of the long period stacking ordered (LPSO) phases, which has never been reported by previous works before. The $Mg_{98.5-x}Zn_{0.5}Y_1Zr_x$ (x =0, 0.1, 0.2 and 0.3 at. %) magnesium alloys were fabricated by directional solidification, and the effects of the Zr content on the distribution characteristics of the bulk LPSO phases (18R) and the lamellar LPSO phases (14H) were investigated. The directional solidification technology showed good controllability in LPSO phase's distribution, and the morphology of LPSO phases in $Mg_{98.5-x}Zn_{0.5}Y_1Zr_x$ (x =0, 0.1, 0.2 and 0.3 at. %) alloys were observed clearly. The results showed that the amount and the morphology of the 14H and 18R LPSO phases within grains continuously decreased with the Zr content increasing. The continuous 14H lamellar structure changed to discontinuous. In addition, Zr element exhibited purification ability on the grain boundaries and refined effect on the 14H and 18R LPSO phases. This can be attributed to the influence of Zr atoms on stacking fault energy (SFE) and the attraction of Zr atoms to Mg atoms.

Keywords: *Mg-Zn-Y magnesium alloys, Long Period Stacking Ordered (LPSO) phases, Stacking Fault Energy (SFE), Zirconium (Zr).*

1. Introduction

In recent years, the high-performance lightweight magnesium alloys have received many attentions in various fields, such as aviation, aerospace, transportations, chemicals, 3C (Computer, Communication and Consumer electronics) and other industries[1-6]. Currently, according to the reports, the consumption of magnesium alloys has increased to the third place as structural material, second only to iron-based and aluminum-based alloys[7]. The ZK60 magnesium alloy is one of the commercial wrought magnesium alloys with high strength. However, ZK60 is still limited in its application due to their poor room temperature ductility compared with commercial aluminum alloys[8-14]. In order to improving the ductility of ZK60 at room temperature, an effective approach is transforming the brittle phase to ductility phase. Therefore, with the addition of rare earth (RE) elements, the brittle Mg-Zn phase can transform to LPSO phases, which exhibit good ductility[15-19]. Furthermore, the RE elements not only purifies the magnesium alloy matrix, but also contribute to refine the grains. In the Mg–M–RE systems (M=Al, Ni, Cu and Zn; RE=Y, Gd, Dy, Ho, Er, Tb and Tm) alloys, LPSO phase would strongly hinder the basic slip system through the formation of the kink binds during the loading and deformation process of the magnesium alloys, thereby RE-magnesium alloys not sacrifice toughness, and keep high strength[20-22]. Generally, 14H and 18R are the most common LPSO phases which in the form of block and lamellar in magnesium alloys, and studies have found that there is a certain orientation relationship between 14H and 18R[23,24]. Due to the similar brick-wall structure between the 14H phase and the magnesium matrix, the breakage of one brick could not cause a wall to collapse. Therefore Mg-Zn-Y system alloys can be expected to be good candidates for high strength and high toughness magnesium alloy materials.

Zr is an essential alloying element for both Mg-Zn and Mg-Zn-Y system alloys. Although the content of Zr in magnesium matrix is very low, its effectively refined effect on Mg grains, so it deserves much attention for many researchers. It is widely accepted that the Zr element can be the powerful nucleant of magnesium and improve the nucleation amount of grains due to the similarity in the lattice parameters between Zr and Mg. However, the trace Zr elements are difficult to find by common ways, there is no direct evidence to prove the refinement mechanism of Zr element in magnesium alloys[25,26]. Not only Zr element has the grain refined effect, but the other effects cannot be ignored as well. Robson and Paa-Rai[27] found that Zr can reduce the amount of aging precipitates and decrease the age hardening effect on magnesium matrix. It is attributed to the precipitation of coarse Zn-Zr phases which inhibit the precipitation of β′-MgZn phase. Because of the lattice distortion releasing and thermal conductivity improving, the solubility content of Zn would decrease significantly with the Zr adding[27,28]. Li et al.[29] investigated the microstructure and thermal conductivity of Mg-2Zn-Zr alloy, they found the main precipitated phases of Mg-2Zn-Zr alloy are Zn_2Zr and Zn_2Zr_3, and they concluded that these phases improved both the thermal conductivity and the strength of Mg-2Zn-Zr

*e-mail: fzxue2003@163.com

alloy. Although the reasons of these effects were not clearly, the fact that the Zr element contributes to improving the mechanical and physical properties of the Mg-Zn series alloys cannot be ignored.

In present work, the Mg-Zn-Y alloys were prepared by direction solidification to control, and the distribution of LPSO phase in Mg-Zn-Y alloys were observed obviously, and the relationship between the content of Zr and the distribution characteristics of LPSO phase were also established in this study. Furthermore, the distribution characteristics of LPSO phases in Mg-Zn-Y alloys changed with the Zr element adding which might prove a new perspective to control the growth process of LPSO phases and provide a new idea for designing high strength and high toughness Mg-Zn-Y system alloys.

2. Experimental

2.1 Material preparation and heat treatments

The master ingots with different nominal composition ($Mg_{98.5-x}Zn_{0.5}Y_1Zr_x$, x =0, 0.1, 0.2 and 0.3 at. %) were prepared by resistance furnace in an argon atmosphere. pure Mg (>99.8%), pure Zn (>99.8%), Mg-25%Y (wt. %) and Mg-25%Zr (wt. %) were used as the raw materials. The ingots were re-melted in a self-manufactured furnace as previously described in Xu et al.[30] and Li et al.[31]. The ingots were putted into stainless steel crucibles with a 28/30 mm diameter (inside/outside diameter) and a length of 165 mm. The directional solidification process was carried out in the argon atmosphere. The specimens were heated to 1003 K over 1h and thermally stabilized for 2 h. After that, turned off the bottom set of resistive wires, cooled the bottom of crucibles by a water-cooled copper base, and then controlled the top set of resistive wires to keep the samples cool with 10 °C/min. At the end of the experiment, when the temperature went down to 673 K, turned off all the power and remained the sample in the furnace until the temperature down to room temperature.

2.2 Microstructural characterizations

The chemical composition of $Mg_{98.5-x}Zn_{0.5}Y_1Zr_x$ (x =0, 0.1, 0.2 and 0.3 at. %) alloys was measured by inductively coupled plasma-atomic emission spectrometry (ICP-AES), as listed in Table 1. The casting samples were mechanically polished and etched with 4% nital, an ethanol solution of picric acid and glacial acetic acid (2.0 g picric acid, 5 ml glacial acetic acid, 5 ml water and 25 ml ethanol). Microstructures of specimens were analyzed by optical microscope (OM) and FEI SIRION 200 scanning electron microscopy (SEM) equipped with an Oxford energy dispersive X-ray spectrometer (EDS). Characterization of LPSO structure was performed in a JEOL JEM 2100F FEGTEM transmission electron microscopy operating at 200 KV.

Table 1. The chemical composition of the as-cast alloy (at. %).

Alloys	Nominal composition	Measured composition			
		Y	Zn	Zr	Mg
A	$Mg_{98.5}Y_1Zn_{0.5}$	0.86	0.42	-	Bal.
B	$Mg_{98.4}Y_1Zn_{0.5}Zr_{0.1}$	0.87	0.44	0.08	Bal.
C	$Mg_{98.3}Y_1Zn_{0.5}Zr_{0.2}$	0.85	0.43	0.16	Bal.
D	$Mg_{98.2}Y_1Zn_{0.5}Zr_{0.3}$	0.89	0.42	0.25	Bal.

2.3 Atomic model and calculation details

The model was built on the super-cell of Mg (a × b × c=5 × 5 × 3, a, b, and c represent directions of Mg crystal lattice respectively). The total number of atoms in super-cell was 150. One Mg atom was replaced by Zr atom. In this study, the fractional coordinates of Zr atom was (0.67, 0.33, 0.50). The crystal structure of the calculation model was showed in Figure 1. Our calculations were performed using the Cambridge Serial Total Energy Package Code (CASTEP) based on DFT. The Generalized Gradient Approximation (GGA) was employed to evaluate exchange-correlation energy. Ultra-soft pseudo-potentials were used for electron-ion interactions and the electron wave function was expanded using plane waves. Mg $2p^63s^2$ and Zr $4s^24p^64d^25s^2$ were treated as valence electrons. The cut-off energy was 380 eV and the K-point was 12 × 12 × 6 to ensure the convergence of the system energy and configuration at the plane wave group level.

2.4 Stacking fault energy calculation method

According to the thermodynamic calculation model of the basal plane stacking fault energy in the hexagonal pure metal, when the stacking fault occurs in close-packed hexagonal metal, the close-packed hexagonal (hcp) of ABABAB…… arrangement in the stacking fault regions are changed to face-centered cubic (fcc) of ……ABABABCBABA…… arrangement in (0001) plane. We characterized the stacking fault energy of magnesium by calculating the energy required for the hcp→fcc structural transformation. In the calculation process, the variables are Zr content and temperature. When the Zr content is selected as the variable to calculate the stacking fault energy, the temperature was fixed to 800K (the most common solid solution temperature[32], the elements in the Mg matrix more inclined to segregation at stacking

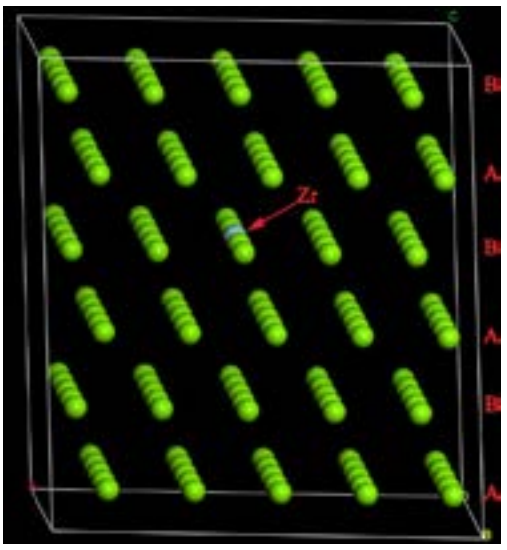

Figure 1. The crystal structure of the calculation model.

fault position, and this facilitates precipitation of the second phase). In addition, the total amount of Mg and Zr elements in the calculation process are regarded as 100%, and the linear relationship is performed by taking the value of Zr content (the value taken distance was divided into 0.0005 at. %). Similarly, when the temperature is selected as the variable, the calculation was performed by Mg-0.2Zr (at. %), and the temperature setting range was from 300K to 900K in the heat treatment temperature range (the value taken distance was divided into 50K).

3. Results

The microstructure of A, B, C and D alloys were showed in Figure 2a-d (a_1-d_1) and Figure 3a-d. It mainly consisted of well-development primary α-Mg and LPSO phases consisted

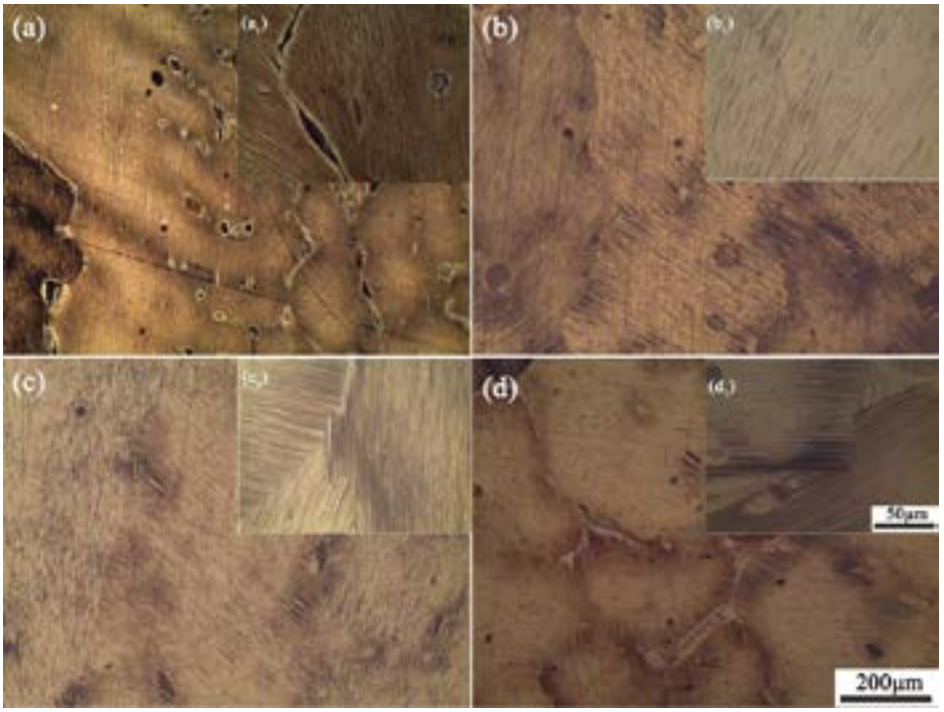

Figure 2. OM images of Mg-Zn-Y magnesium alloys with different content of Zr: (a) A alloy; (b) B alloy. (c) C alloy; (d) D alloy; (a_1), (b_1), (c_1) and (d_1) were zoom in of images (a), (b), (c), and (d), respectively.

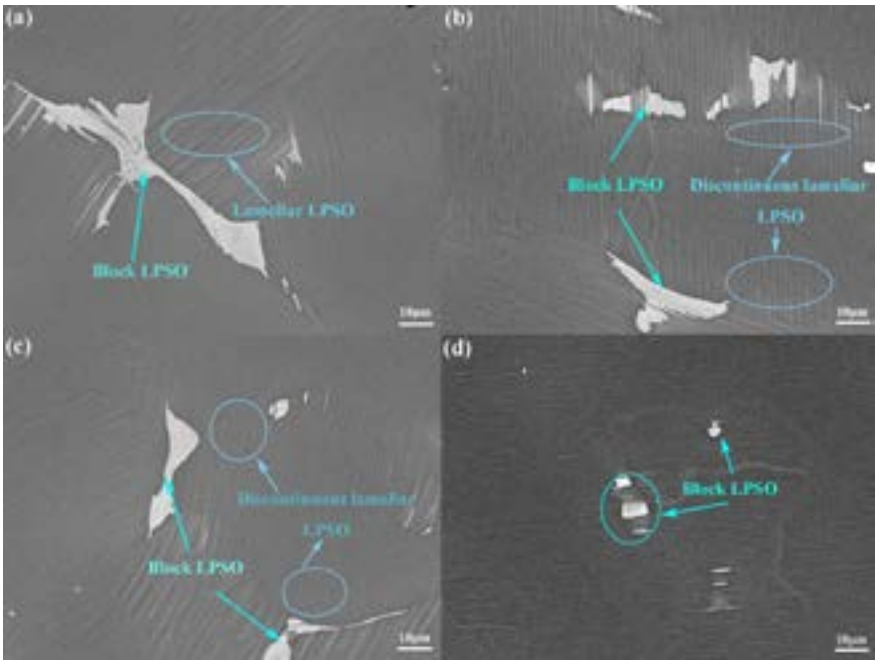

Figure 3. Typical SEM images of Mg-Zn-Y magnesium alloys with different content of Zr: (a) A alloy; (b) B alloy; (c) C alloy; (d) D alloy.

by the bulk phases and the lamellar structure phases. The bulk phases in the grain boundary were 18R LPSO phases and the lamellar structures within grains were 14H LPSO phases, as shown in Figure 2a-d (a_1-d_1). The crystal structure of the lamellar structure LPSO phases and the microstructure in the A alloy was examined by TEM, as shown in Figure 4a, b and Figure 5. The type of the bulk phases and the lamellar phases was also identified in detail in our previous study[30,33]. As seen in Figure 2, the changes of distribution characteristics of LPSO phases in A, B, C and D alloys were clearly observed in this study. Figure 2 (a, a_1) presented that the 14H LPSO phases were parallel along their longitudinal axis within grains, and showed obvious orientation. The 14H LPSO phases in the B alloy were finer than the A alloy and the continuous lamellar structure changed to discontinuous, as showed in Figure 2 (b, b_1). Additionally, the grain boundary was broad and some bulk phases appeared in the grain boundary, as showed in the Figure 2a. However, in the B, C, and D alloys, the grain boundary became finer and cleaner than the A alloy, as showed in Figure 2b-d. These findings demonstrated that Zr have a purity effect on grain boundary and affect the morphology and distribution of 14H and 18R as well. With increasing the content of Zr from 0.1 to 0.2 at. %, the amount and the size of the 14H LPSO phases were continuously decreasing, as showed in Figure 3a-c. Particularly, when the Zr element was adding to 0.3 at. %, most of the 14H LPSO phases disappeared, there were almost no 14H LPSO phases in Mg matrix. Similarly, the 18R phase has same trend in morphology and amount compared with 14H, and it showed that the bulk 18R phases are finer and more dispersed with the Zr content increasing, as shown in Figure 3a-d. This further proved that Zr had an influence on the distribution characteristic of the 14H phases and 18R phases. Furthermore, due to the difference between A, B, C, and D alloys, this suggested that the addition of Zr would break the balance of 14H and 18R which are presented in Figure 3b-d.

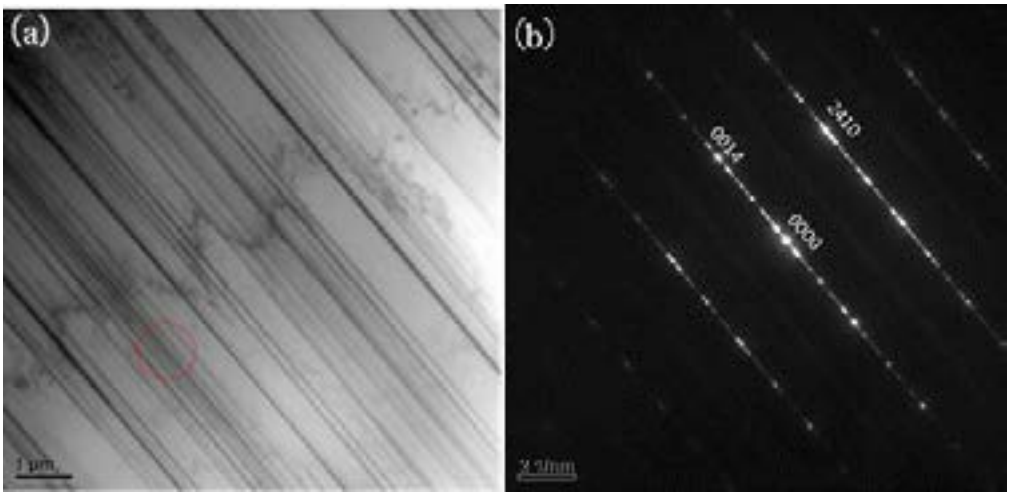

Figure 4. (a) The bright-field TEM image of the $Mg_{98.5}Zn_{0.5}Y_1$ alloy; (b) The $[10\bar{3}0]$ Selected Area Electron Diffraction (SAED) of the lamellar structure phase (indicated by red circle in (a)).

Figure 5. HRTEM images of the microstructures of the $Mg_{98.5}Zn_{0.5}Y_1$ matrix and lamellar structure.

4. Discussion

From the results obtained in the present study, two important conclusions can be concluded. Firstly, adding Zr elements beneficially refine the 14H LPSO and 18R LPSO phases. With the content of Zr increasing from 0.1 at. % to 0.3 at. %, the amount and the size of the 14H LPSO phases within grains continuously decreased. The discontinuous lamella was similar to the 14H LPSO phase in the Mg-2.0Gd-1.2Y-Zn-0.2Zr (at. %) alloy reported by Honma et al.[34]. When Zr content increasing to 0.3 at. %, a few bulk phases would occur in the grain, as showed in Figure 3b-d. Secondly, Zr had a significant purity and refine effect on the grain boundary. The grain boundary became finer and cleaner than those without Zr adding. Based on above discussions, a four-step microstructure evolution mechanism can be established, and the schematic illustration was proposed in Figure 6, and the main reason can be summarized as follows:

When Zr adding to the $Mg_{98.5}Zn_{0.5}Y_1$ alloy, the change of SFE play an important role in decreasing the amount of 14H and 18R LPSO phase. According to previous reports, the formation processes of the LPSO phases were close connected with the SFE of the matrix[33,35-37]. In order to understand the effect of the Zr content on the distribution characteristic of the LPSO phases, the SFE of the magnesium matrix with different Zr content are calculated as following equation[38,39]:

$$\gamma = \frac{1}{N_0^{1/3} V^{2/3}} \left(\sum_i^n X_i \Delta G_i^{\alpha \to \beta} + \frac{1}{2} \sum_i^n \sum_j^n \Delta W_{ij}^{\alpha \to \beta} X_i X_j \right) \quad (1)$$

where N_0 is Avogadro constant and V is molar volume of alloys. $\Delta G_i^{\alpha \to \beta}$ is free energy change of the structure transition of 'i' element. X_i and X_j is the molar fraction of 'i' and 'j' element, respectively. $\Delta W_{ij}^{\alpha \to \beta}$ is the interaction factors between 'i' and 'j' element $(i \neq j)$ in the process of structural transformation.

This equation was deduced and proved in our previous works[38,39]. Table 2 showed the numerical values and functions used for the thermodynamic calculations. The calculation results were illustrated in Figure 7. According to the results,

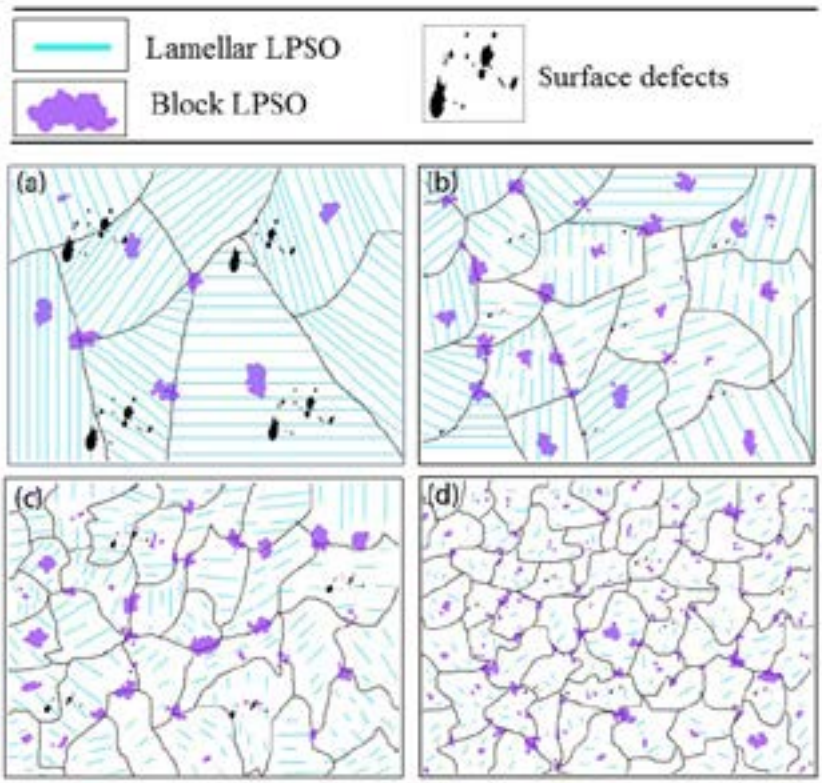

Figure 6. Schematic illustration for microstructure evolution of (a) A alloy; (b) B alloy; (c) C alloy; (d) D alloy.

Table 2. Numerical values and functions used for the thermodynamic calculations.

parameter	$\Delta G_i^{\alpha \to \beta} = a_i + b_i T$			$^{k}L_{ij}^{\alpha \to \beta} = a_{ij} + {}^{k}b_{ij} T$			$\Delta W_{ij}^{\alpha \to \beta} = A_{ij} + B_{ij} T$	
	a_i	b_i		a_{ij}	$^{k}b_{ij}$		A_{ij}	B_{ij}
$\Delta G_{Mg}^{\alpha \to \beta}$	2500.000	-0.900	$^{k}L_{Mg,Zr}^{\alpha \to \beta}$	-10872.000	18.093	$\Delta W_{Mg,Zr}^{\alpha \to \beta}$	-10.839	0.018
$\Delta G_{Zr}^{\alpha \to \beta}$	7302.056	-0.703						

Note: α→β represents the energy difference between the two structures of hcp and fcc

the tendency of SFE increase with the atomic percent of Zr increasing, as shown in Figure 7a. This suggested that adding Zr element could increase SFE. Conversely, with the temperature increasing, the value of SFE reduced, as shown in Figure 7b, and the lower SFE could benefit to generate LPSO phases. This was the main reason why the LPSO phase was much easier to grow during directional solidification process.

However, the SFE not increased sharply with the atomic percent of Zr increasing. This result did not match the obviously change of the 14H and 18R LPSO phases morphology and could not explain why the continuous lamellar structure 14H LPSO phase changed into discontinuous. There should be another reason for influence the forming process of the 14H and 18R LPSO phases. In order to investigating the reason of the 14H and 18R LPSO phases distribution characteristics with Zr element adding, the electron density between Mg and Zr atoms was calculated by first principle. The electron density of (001) lattice plane was showed in Figure 8. It can be found that the electron density around Zr atom was higher than Mg atoms and exhibited locality property. The higher electron density would increase the attractive force between Zr atoms and Mg atoms. Because the stacking fault energy in magnesium matrix changed the atomic arrangement from ABAB to ABCABC[39], so the attractive force between Zr atoms and Mg atoms increasing would increase the local energy consumed by misplacing atomic layers and obstruct the diffusion of elements. This would improve the energy barrier for generating 14H and 18R, and break the growth channel of the 14H LPSO phases. Finally, causing the continuous lamellar structure to discontinuous. These results further explained the change of distribution characteristics of LPSO phase with adding trace content of Zr, even though SFE not increased obviously.

Besides that, because both of the Zr atoms and Mg atoms are hexagonal close packed lattice, the magnesium matrix could accept Zr element without severely energy increasing and crystal lattice distortion in the process of Zr adding. Therefore, there is not obviously energy difference between the Zr atoms located in grains and grain boundaries, unlike the common eutectic elements Al, Ca, and Si, the segregation of Zr atoms in the grain boundaries are not easy to occur, and this keeps the entire system of the Mg-Zn-Y-Zr matrix in the lowest energy state. Meanwhile, Zr element could increase the attractive force between Zr atoms and Mg atoms, this force stimulates the bond between grains more tightly. These factors could contribute to the grain boundaries finer and cleaner. In addition, because the finer and cleaner grain boundaries represent more stable energy and less energy fluctuations, the energy of nucleation and growth of the 14H and 18R phases increases. This would reduce the bulk and lamellar structure in the grain.

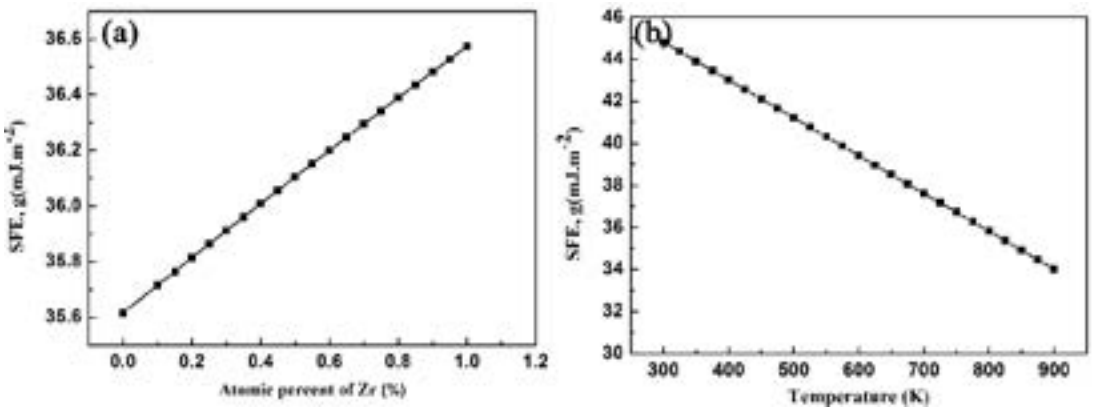

Figure 7. (a) Stacking fault energy (SFE) of Mg matrix with different content of Zr; (b) SFE of Mg-0.2Zr (at. %) at different temperature.

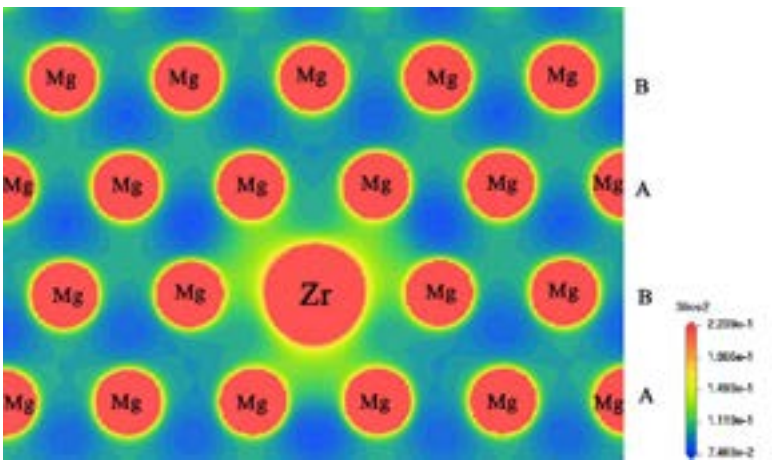

Figure 8. Electron density of (0 0 1) lattice plane.

5. Conclusions

1. The amount and the morphology of the 14H LPSO phases within grains continuously decreased, and the continuous lamellar structure within grains transform to discontinuous with the Zr content increasing to 0.1 at. % and 0.2 at. %. In addition, the bulk 18R phases are finer and more dispersed when Zr content adding to 0.3 at. %.
2. In B, C and D alloys, the grain boundaries are finer and cleaner than the A alloy. This can be attributed to the fact that the addition of the Zr element reduced the energy of the matrix and grain boundaries of the Mg-Zn-Y alloy.
3. According to the calculation results, Zr element would increase the SFE of magnesium alloy, then increase the energy of nucleation and growth of bulk phases and the lamellar phase, and cause the amount of 14H and 18R LPSO phases decreasing. Furthermore, because the Zr atom would increase the attractive force between Zr-Mg atoms, this would break the growth channel of the lamellar structure and change the continuous lamellar structure to discontinuous.

6. Acknowledgements

This work was supported by the Yunnan Province Science Youth Experts Fund [2016FD033].

7. References

1. Joost WJ, Krajewski PE. Towards magnesium alloys for high-volume automotive applications. Scr Mater. 2017;128:107-12. http://dx.doi.org/10.1016/j.scriptamat.2016.07.035.
2. Chen X, Liu J, Pan F. Enhanced electromagnetic interference shielding in ZK60 magnesium alloy by aging precipitation. J Phys Chem Solids. 2013;74(6):872-8. http://dx.doi.org/10.1016/j.jpcs.2013.02.003.
3. Xianhua C, Yuxiao G, Fusheng P. . Research progress in magnesium alloys as functional materials. Rare Met Mater Eng. 2016;45(9):2269-74. http://dx.doi.org/10.1016/S1875-5372(17)30015-2.
4. Esmaily M, Svensson JE, Fajardo S, Birbilis N, Frankel GS, Virtanen S, et al. Fundamentals and advances in magnesium alloy corrosion. Prog Mater Sci. 2017;89:92-193. http://dx.doi.org/10.1016/j.pmatsci.2017.04.011.
5. Radha R, Sreekanth D. Insight of magnesium alloys and composites for orthopedic implant applications – a review. J. Magn. Alloys. 2017;5(3):286-312. http://dx.doi.org/10.1016/j.jma.2017.08.003.
6. Wang XJ, Xu DK, Wu RZ, Chen XB, Peng QM, Jin L, et al. What is going on in magnesium alloys? J Mater Sci Technol. 2017;7:1-3. http://dx.doi.org/10.1016/j.jmst.2016.11.017.
7. Samaniego A, Gusieva K, Llorente I, Feliu S Jr, Birbilis N. Exploring the possibility of protective surface oxides upon Mg alloy AZ31 via lutetium additions. Corros Sci. 2014;89:101-10. http://dx.doi.org/10.1016/j.corsci.2014.08.015.
8. Chen XR, Ning FK, Hou J, Le QC, Tang Y. Dual-frequency ultrasonic treatment on microstructure and mechanical properties of ZK60 magnesium alloy. Ultrason Sonochem. 2018;40(Pt A):433-41. http://dx.doi.org/10.1016/j.ultsonch.2017.07.027. PMid:28946443.
9. Hadadzadeh A, Wells MA. Analysis of the hot deformation of ZK60 magnesium alloy. J Magn Alloys. 2017;5(4):369-87. http://dx.doi.org/10.1016/j.jma.2017.09.002.
10. Ciccarelli D, El Mehtedi M, Jager A, Spigarelli S. Analysis of flow stress and deformation mechanism under hot working of ZK60 magnesium alloy by a new strain-dependent constitutive equation. J Phys Chem Solids. 2015;87:183-95. http://dx.doi.org/10.1016/j.jpcs.2015.08.020.
11. Karparvarfard SMH, Shaha SK, Behravesh SB, Jahed H, Williams BW. Microstructure, texture and mechanical behavior characterization of hot forged cast ZK60 magnesium alloy. J Mater Sci Technol. 2017;33(9):907-18. http://dx.doi.org/10.1016/j.jmst.2017.04.004.
12. Kim B, Baek SM, Lee JG, Park SS. Enhanced strength and plasticity of Mg-6Zn-0.5Zr alloy by low-temperature indirect extrusion. J Alloys Compd. 2017;706:56-62. http://dx.doi.org/10.1016/j.jallcom.2017.02.206.
13. Yang Y, Jiang LH. Self-organization of adiabatic shear bands in ZK60 Magnesium alloy. Mater Sci Eng. 2016;655:321-30. http://dx.doi.org/10.1016/j.msea.2016.01.008.
14. Yang Y, Wang Z, Jiang LH. Evolution of precipitates in ZK60 magnesium alloy during high strain rate deformation. J Alloys Compd. 2017;705:566-71. http://dx.doi.org/10.1016/j.jallcom.2017.02.158.
15. Wang Y, Zhang Y, Gao W. Effect of Zr on the microstructures and mechanical properties of as-extruded Mg-2.3Zn-0.18Y-xZr alloys. Int J Mod Phys B. 2017;31(16-19):1744001. http://dx.doi.org/10.1142/S0217979217440015.
16. Luo SQ, Tang AT, Pan FS, Song K, Wang WQ. Effect of mole ratio of Y to Zn on phase constituent of Mg-Zn-Zr-Y alloys. Trans Nonferrous Met Soc China. 2011;21(4):795-800. http://dx.doi.org/10.1016/S1003-6326(11)60783-8.
17. Shahzad M, Waqas H, Rafi-ud-din, Qureshi AH, Wagner L. d. Rafi ud, A.H. Qureshi, L. Wagner, The roles of Zn distribution and eutectic particles on microstructure development during extrusion and anisotropic mechanical properties in a Mg–Zn–Zr alloy. Mater Sci Eng A. 2015;620:50-7. http://dx.doi.org/10.1016/j.msea.2014.09.109.
18. Chen Q, Lin J, Shu DY, Hu CK, Zhao ZD, Kang F, et al. Microstructure development, mechanical properties and formability of Mg-Zn-Y-Zr magnesium alloy. Mater Sci Eng. 2012;554:129-41. http://dx.doi.org/10.1016/j.msea.2012.06.025.
19. Yang X, Wu SS, Lu SL, Hao LY, Fang XG. Refinement of LPSO structure in Mg-Ni-Y alloys by ultrasonic treatment. Ultrason Sonochem. 2018;40(Pt A):472-9. http://dx.doi.org/10.1016/j.ultsonch.2017.07.042. PMid:28946448.
20. Yokobayashi H, Kishida K, Inui H, Yamasaki M, Kawamura Y. Enrichment of Gd and Al atoms in the quadruple close packed planes and their in-plane long-range ordering in the long period stacking-ordered phase in the Mg–Al–Gd system. Acta Mater. 2011;59(19):7287-99. http://dx.doi.org/10.1016/j.actamat.2011.08.011.
21. Yang Q, Guan K, Li B, Meng F, Lv S, Yu Z, et al. Coexistence of 14H and 18R-type long-period stacking ordered (LPSO) phases following a novel orientation relationship in a cast Mg−Al−RE−Zn alloy. J Alloys Compd. 2018;766:902-7. http://dx.doi.org/10.1016/j.jallcom.2018.07.053.
22. Lv S, Li Y, Lü X, Meng F, Yang Q, Han D, et al. The types and structures of the intermetallic phases in a cast Mg−4Al−15Gd−4Y−1Zn alloy. J Alloys Compd. 2018;731:612-9. http://dx.doi.org/10.1016/j.jallcom.2017.10.093.
23. Hagihara K, Li Z, Yamasaki M, Kawamura Y, Nakano T. Strengthening mechanisms acting in extruded Mg-based long-period stacking ordered (LPSO)-phase alloys. Acta Mater. 2019;163:226-39. http://dx.doi.org/10.1016/j.actamat.2018.10.016.
24. Guan K, Meng F, Qin P, Yang Q, Zhang D, Li B, et al. Effects of samarium content on microstructure and mechanical properties of Mg–0.5Zn–0.5Zr alloy. J Mater Sci Technol. 2019;35(7):1368-77. http://dx.doi.org/10.1016/j.jmst.2019.01.019.
25. Lee YC, Dahle AK, StJohn DH. The role of solute in grain refinement of magnesium. Metall Mater Trans, A Phys Metall

Mater Sci. 2000;31(11):2895-906. http://dx.doi.org/10.1007/BF02830349.
26. StJohn DH, Qian M, Easton MA, Cao P, Hildebrand Z. Grain refinement of magnesium alloys. Metall Mater Trans, A Phys Metall Mater Sci. 2005;36(7):1669-79. http://dx.doi.org/10.1007/s11661-005-0030-6.
27. Robson JD, Paa-Rai C. The interaction of grain refinement and ageing in magnesium–zinc–zirconium (ZK) alloys. Acta Mater. 2015;95:10-9. http://dx.doi.org/10.1016/j.actamat.2015.05.012.
28. Elsayed A, Sediako D, Ravindran C. Solidification Behavior of Mg-Zn and Mg-Zn-Zr Alloys Using In-Situ Neutron Diffraction. J Mater Eng Perform. 2015;24(6):2250-5. http://dx.doi.org/10.1007/s11665-015-1497-y.
29. Li B, Hou L, Wu R, Zhang J, Li X, Zhang M, et al. Microstructure and thermal conductivity of Mg-2Zn-Zr alloy. J Alloys Compd. 2017;722(Suppl. C):772-7. http://dx.doi.org/10.1016/j.jallcom.2017.06.148.
30. Xu Z, Feng Z, Shi Q, Yang Y, Wang X. The microstructure of Mg98.5Zn0.5Y1 Alloy with long-period stacking ordered structure. Mater Trans. 2017;58(6):862-7. http://dx.doi.org/10.2320/matertrans.M2016440.
31. Li FB, Feng ZX, Cao Y, Shi QN. Research of impurity phase in single crystal pure magnesium prepared by directional solidification. Special Casting & Nonferrous Alloys. 2015;35(2):208-11.
32. Wu YJ, Zeng XQ, Lin DL, Peng LM, Ding WJ. The microstructure evolution with lamellar 14H-type LPSO structure in an Mg96.5Gd2.5Zn1 alloy during solid solution heat treatment at 773K. J Alloys Compd. 2009;477(1):193-7. http://dx.doi.org/10.1016/j.jallcom.2008.10.126.
33. Luo S. Experimental and theoretical investigation of solid solution strengthening and second phase strengthening in Mg-Zn-Zr-Y alloys [dissertation]. Chongqing: Chongqing University; 2011.
34. Honma T, Ohkubo T, Kamado S, Hono K. Effect of Zn additions on the age-hardening of Mg–2.0Gd–1.2Y–0.2Zr alloys. Acta Mater. 2007;55(12):4137-50. http://dx.doi.org/10.1016/j.actamat.2007.02.036.
35. Liu H, Yan K, Yan J, Xue F, Sun J, Jiang J, et al. Precipitation behavior of 14H LPSO structure in single 18R phase Mg–Y–Zn alloy during annealing at 773 K. Trans Nonferrous Met Soc China. 2017;27(1):63-72. http://dx.doi.org/10.1016/S1003-6326(17)60007-4.
36. Pan F-s, Luo S-q, Tang A-t, Peng J, Lu Y. Influence of stacking fault energy on formation of long period stacking ordered structures in Mg–Zn–Y–Zr alloys, Prog. Nat. Sci-Mater. 2011;21(6):485-90.
37. Umantsev A, Ode M. Formation of long-period stacking fault structures in magnesium alloys. Comput Mater Sci. 2016;124(Suppl. C):173-82. http://dx.doi.org/10.1016/j.commatsci.2016.07.035.
38. Feng ZX, Zhang XY, Pan FS. Influence of solute and solute segregation on the stacking fault energy in HCP metals. Rare Met Mater Eng. 2012;41(10):1765-9.
39. Feng ZX, Zhang XY, Pan FS. Thermodynamic model for the influence of temperature on the stacking fault energy in HCP metals. Rare Met Mater Eng. 2012;41(9):1638-41.